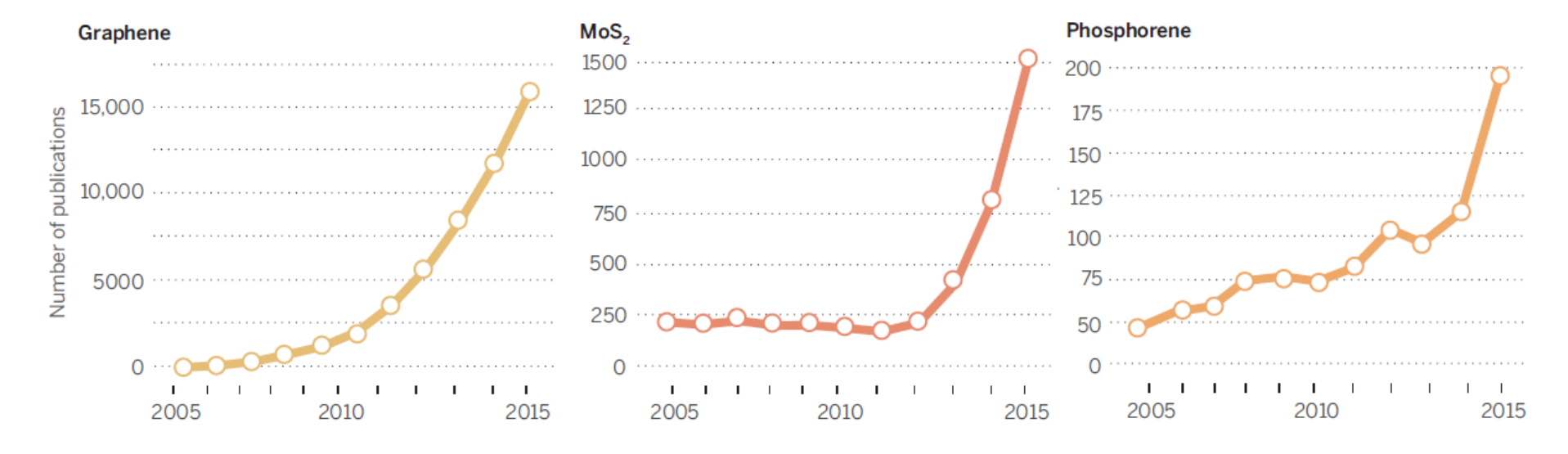
Transition Metal Dichalcogenides (TMDs) MoS_2 and more

The rise of the flattest materials

The number of papers on graphene has grown exponentially since the material was isolated in 2004. Publications about molybdenum disulfide (MoS_2) and phosphorene are now repeating the pattern.



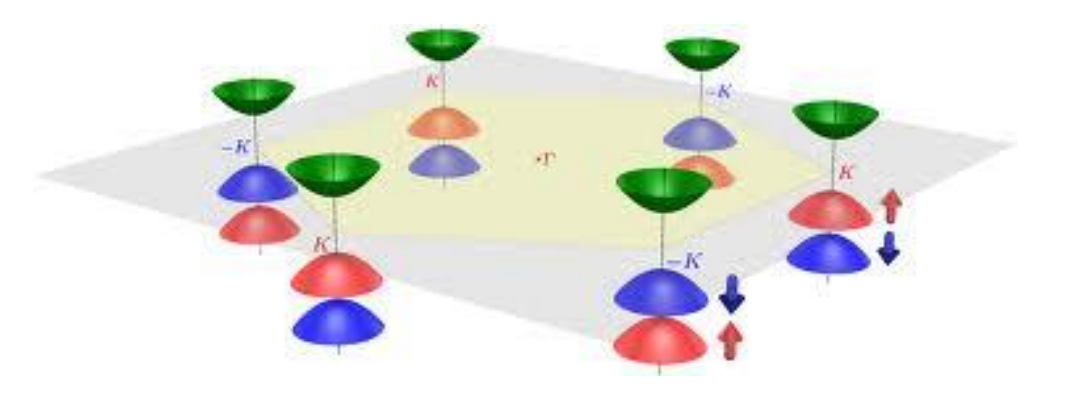
Transition Metal Dichalcogenides (TMDs)

Formula: MX₂ M (transition metals) X (chalcogenides)

```
Mo, W, Nb, Re, Ti, Ta, etc.S, Se, or Te
```

Semiconducting TMDs

- Semi-metal: TiS₂
- Charge-density-wave (CDW)
- Superconductivity: i.e. MoS₂ Appl. Phys. Lett. 101, 042603 (2012);
- Metal-Insulator Transition (http://arxiv.org/abs/1301.4947)
- Valleytronics, involves channeling the charge carriers into "valleys" of set momentum in a controlled way.



Motivation

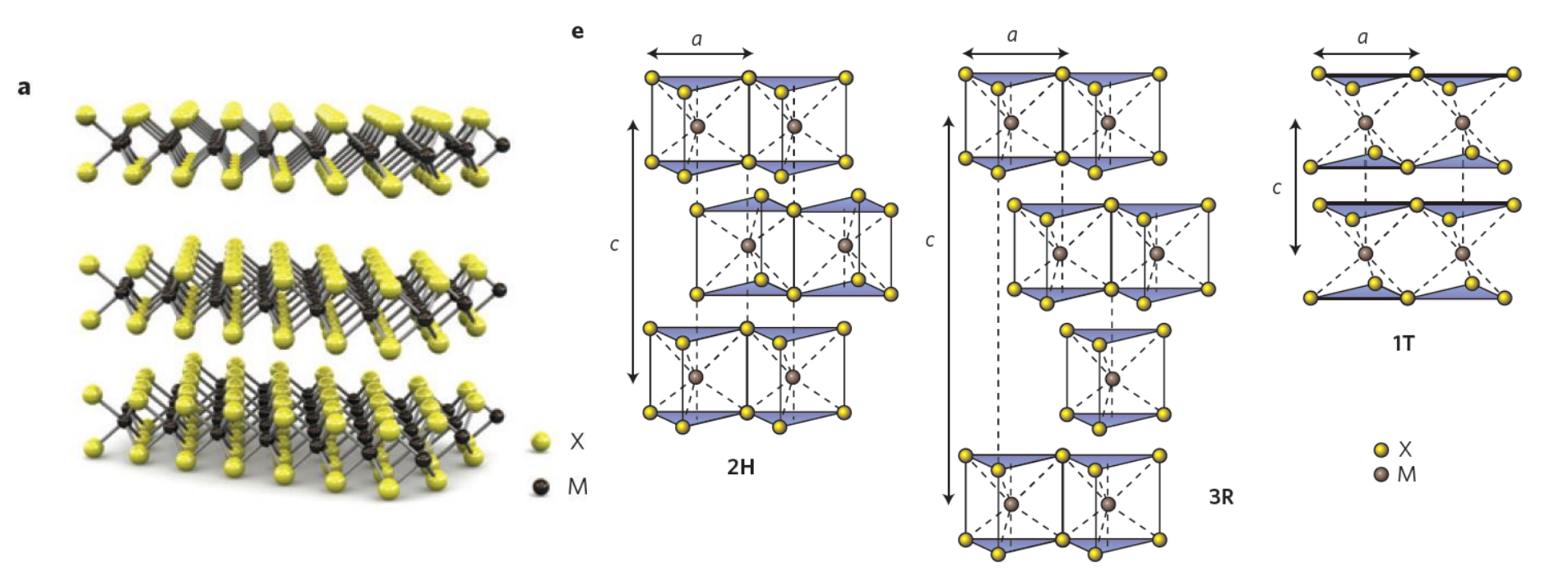
1. Why TMDs?

- A 2D semiconducting transition metal dichalcogenides with potential applications that could complement those of <u>Graphene</u>.
 - High on/off ratio and moderate mobility: electronics
 - Direct bandgap (for monolayer): optoelectronics
 - Valleytronics
- Large area vapor phase growth accessible (so far MoS₂)

2. Bandgap Engineering

- Layer numbers (quantum confinement)
- Strain
- Temperature
- Potentially leads to many optoelectronics applications.

Introduction: TMDc Monolayer



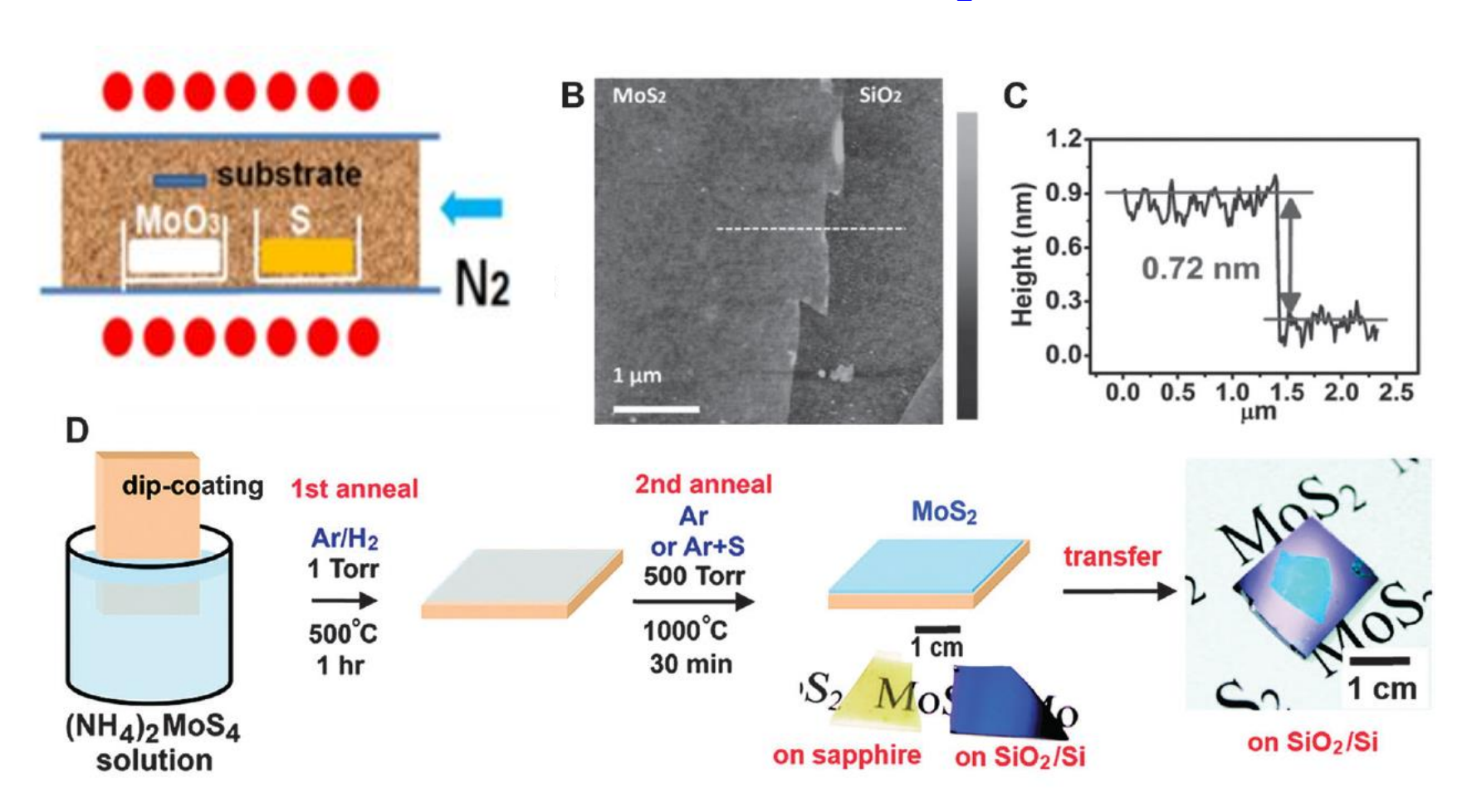


Schematics of the structural polytypes:

- 2H (hexagonal symmetry, two layers per repeat unit, trigonal prismatic coordination),
- 3R (rhombohedral symmetry, three layers per repeat unit, trigonal prismatic coordination), and
- 1T (tetragonal symmetry, one layer per repeat unit, octahedral coordination).

Andras Kis, Nature Nanotech, Vol 6, No 3, 146, (2011).

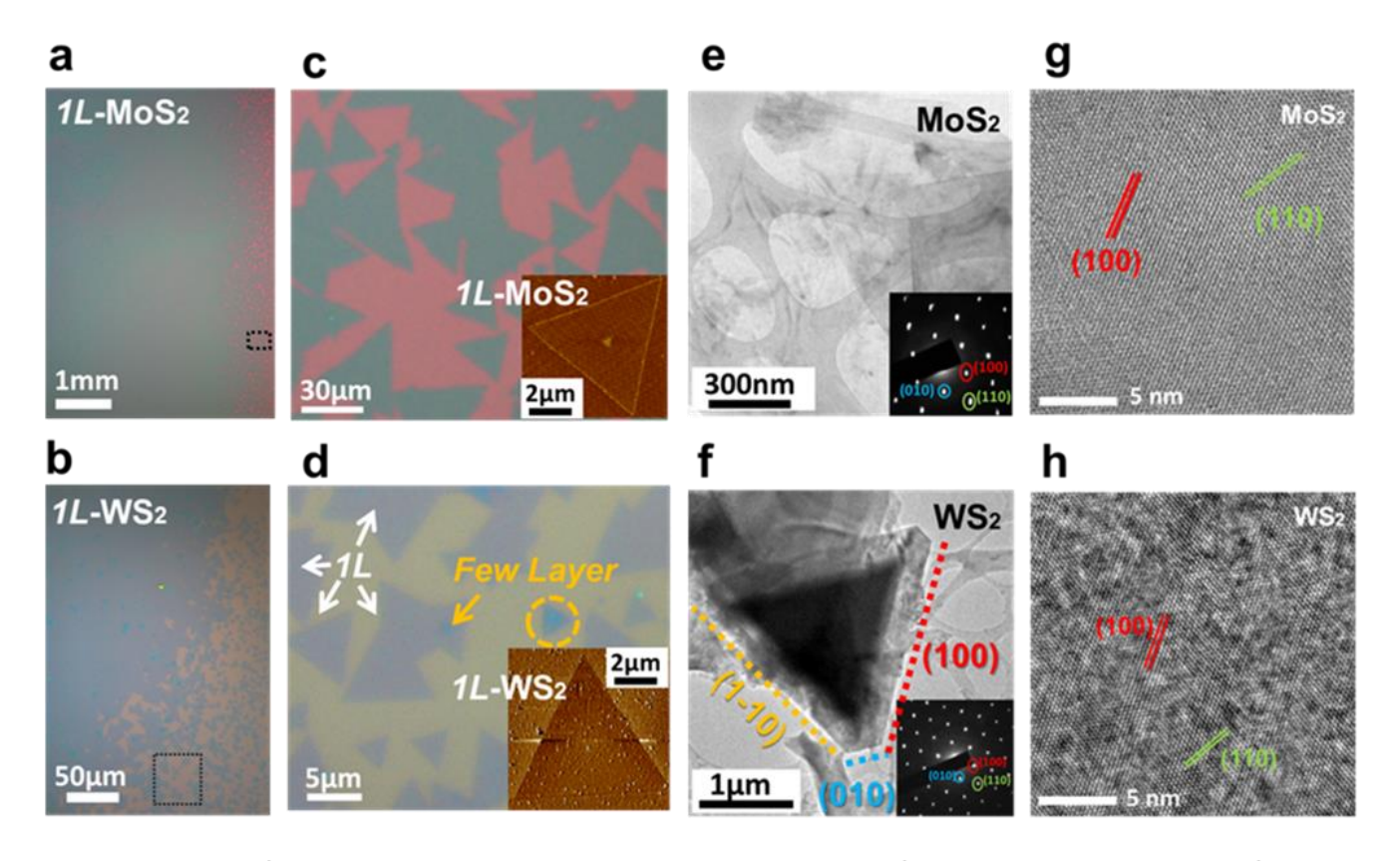
Schematic illustration of the experimental set-up for CVD-growth of MoS₂



Y. H. Lee et al., Adv. Mater. 24, 2320 (2012). Keng-Ku Liu et al., Nano Lett. 12, 1538 (2012).

Synthesis: the thinnest semiconductors, TMD Monolayer

- Scalable,
- Single Crystal
- Thinnest semiconductors



Synthesis of Single Layer Transition Metal Disulfides on Diverse Surfaces

YHLee et. al., *Nano Lett*. 13, 1852–1857 (2013) YHLee et. al, *Adv. Mater*. 24, 2320-2325 (2012)

Atomically Thin MoS₂: A New Direct-Gap Semiconductor

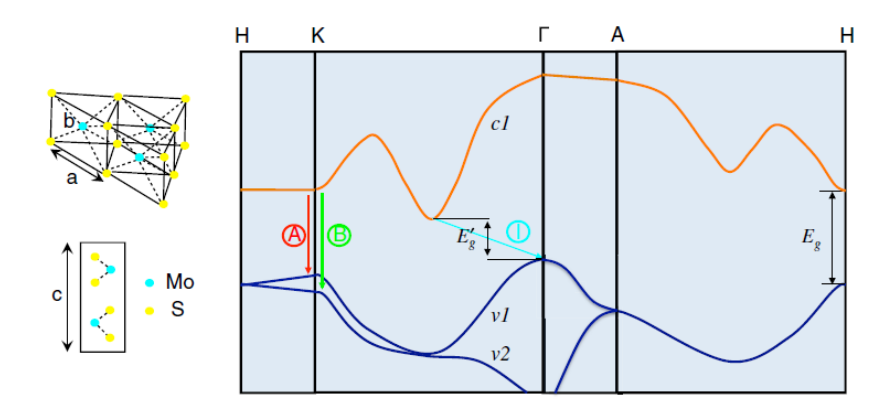


FIG. 1 (color online). Lattice structure of MoS_2 in both the inand out-of-plane directions and simplified band structure of bulk MoS_2 , showing the lowest conduction band c1 and the highest split valence bands v1 and v2. A and B are the direct-gap transitions, and I is the indirect-gap transition. E'_g is the indirect gap for the bulk, and E_g is the direct gap for the monolayer.

K. F. Mak, T. Heinz, PRL 105, 136805 (2010)

- Via optical absorption, photoluminescence, and photoconductivity spectroscopy, the effect of quantum confinement of MoS₂ is traced.
- This leads to a crossover to a direct-gap material in the limit of the single monolayer.
- The freestanding monolayer exhibits an increase in luminescence quantum efficiency by more than a factor of 10⁴ compared with the bulk material.

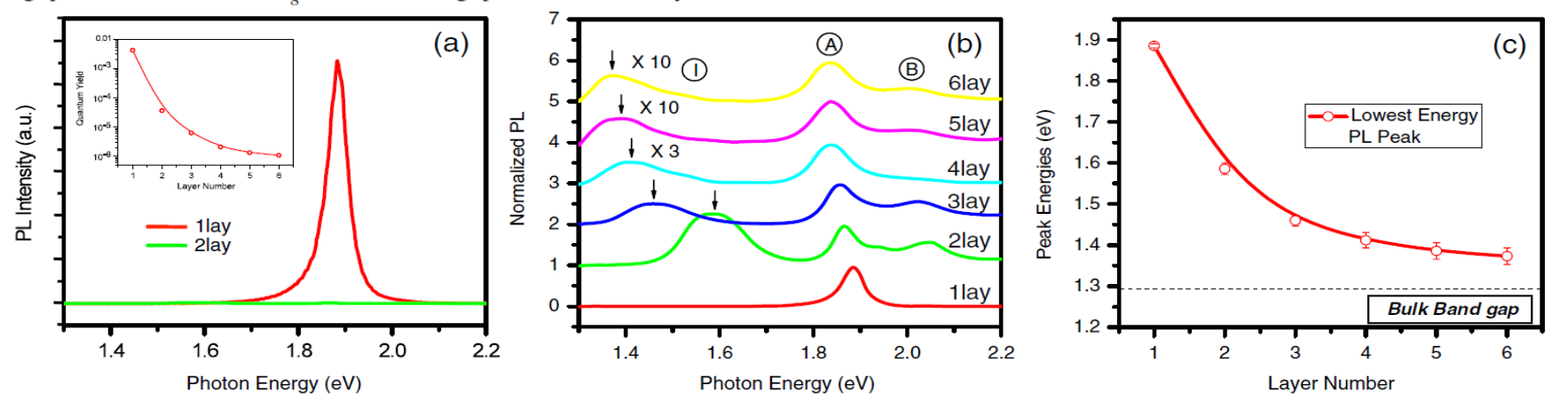
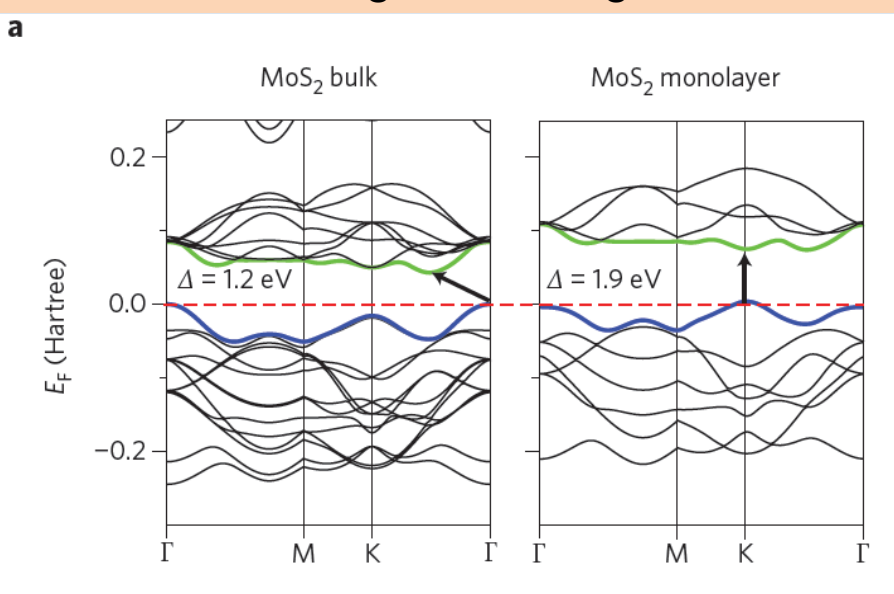


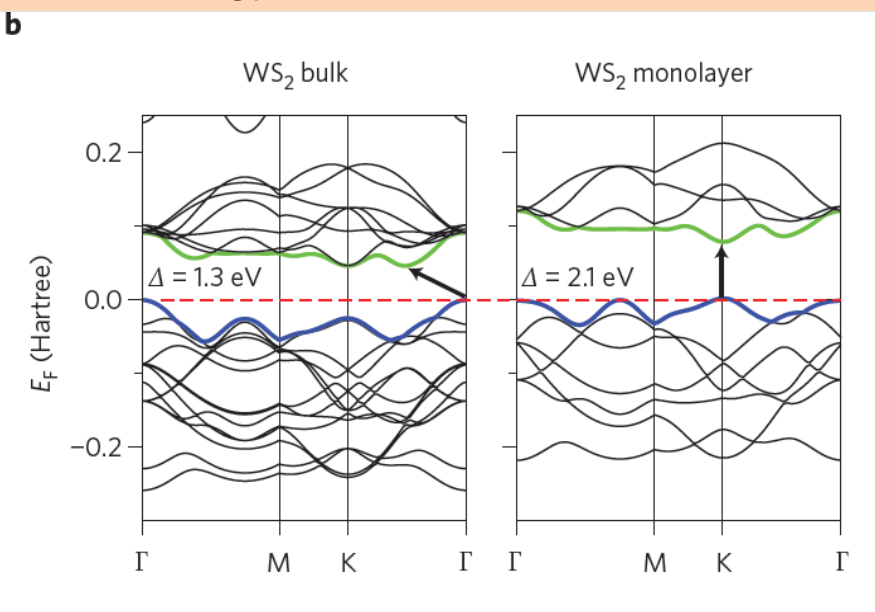
FIG. 3 (color online). (a) PL spectra for mono- and bilayer MoS_2 samples in the photon energy range from 1.3 to 2.2 eV. Inset: PL QY of thin layers for N = 1-6. (b) Normalized PL spectra by the intensity of peak A of thin layers of MoS_2 for N = 1-6. Feature I for N = 4-6 is magnified and the spectra are displaced for clarity. (c) Band-gap energy of thin layers of MoS_2 , inferred from the energy of the PL feature I for N = 2-6 and from the energy of the PL peak A for N = 1. The dashed line represents the (indirect) band-gap energy of bulk MoS_2 .

Table 1 | Summary of TMDC materials and properties.

	- S ₂		-Se₂			-Te ₂	
	Electronic characteristics	References	Electronic characteristics	References	Electronic characteristics	References	
Nb	Metal; superconducting; CDW	138 (E)	Metal; superconducting; CDW	138,164 (E)	Metal	83 (T)	
Та	Metal; superconducting; CDW	138,164 (E)	Metal; superconducting; CDW	138,164 (E)	Metal	83 (T)	
Мо	Semiconducting 1L: 1.8 eV Bulk: 1.2 eV	31 (E) 88 (E)	Semiconducting 1L: 1.5 eV Bulk: 1.1 eV	82 (T) 88 (E)	Semiconducting 1L: 1.1 eV Bulk: 1.0 eV	82 (T) 165 (E)	
W	Semiconducting 1L: 2.1eV 1L: 1.9 eV	25 (T) 82 (T)	Semiconducting 1L: 1.7 eV	83 (T)	Semiconducting 1L: 1.1 eV	83 (T)	
	Bulk: 1.4 eV	88 (E)	Bulk: 1.2 eV	88 (E)			

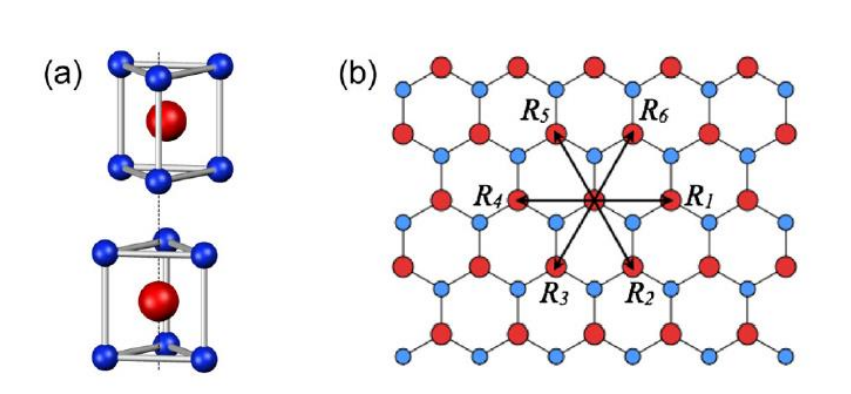
Qing Hua Wang et al., Nature Nanotechnology, 7, 699, (2012).





Coupled Spin and Valley Physics in MoS₂

- □ Inversion symmetry breaking, together with strong SOC, lead to coupled spin and valley physics in monolayer MoS₂ and other group-VI dichalcogenides, making possible spin and valley control in these 2D materials.
- ☐ First, the valley Hall effect is accompanied by a spin Hall effect in both electron-doped and hole-doped systems.
- Second, spin and valley relaxation are suppressed at the valence-band edges, as flip of each index alone is forbidden by the valley-contrasting spin splitting (0.1–0.5 eV) caused by inversion symmetry breaking.
- ☐ Third, the valley-dependent optical selection rule also becomes spin-dependent, and carriers with various combination of valley and spin indices can be selectively excited by optical fields of different circular polarizations and frequencies.
- ☐ We predict photo-induced charge Hall, spin Hall and valley Hall effects.



Di Xiao et al, PRL 108, 196802 (2012)

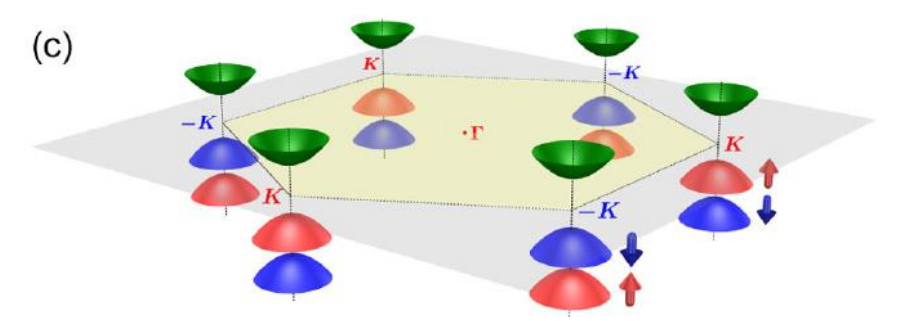
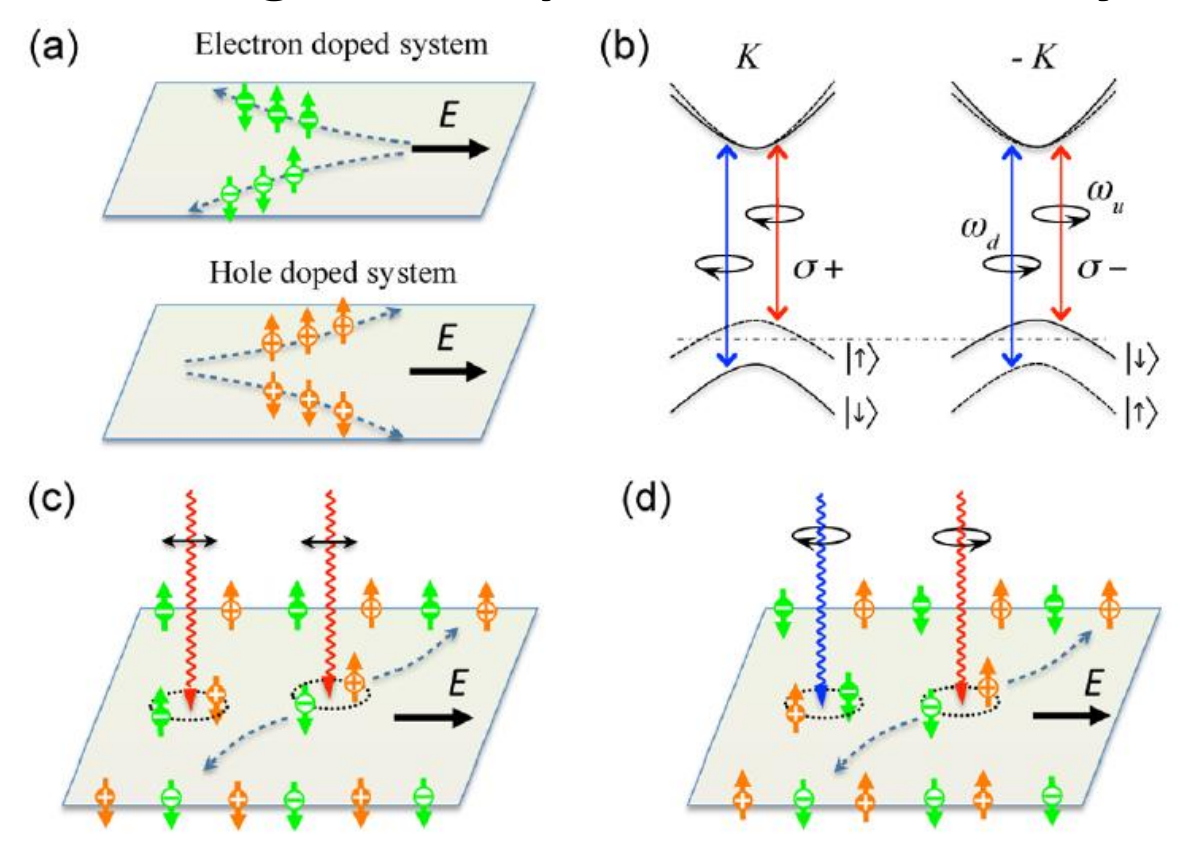


FIG. 1 (color online). (a) The unit cell of bulk 2H-MoS₂, which has the inversion center located in the middle plane. It contains two unit cells of MoS₂ monolayers, which lacks an inversion center. (b) Top view of the MoS₂ monolayer. R_i are the vectors connecting nearest Mo atoms. (c) Schematic drawing of the band structure at the band edges located at the K points.

Photo-induced charge Hall, spin Hall, and valley Hall effects



Coupled spin and valley physics in monolayer group-VI dichalcogenides.

The electrons and holes in valley K are denoted by white '+', and '-' symbol in dark circles and their counterparts in valley – K are denoted by inverse color. (a) Spin Hall effects in electron and hole-doped systems. (b) Valley and spin optical transition selection rules. Solid (dashed) curves denote bands with spin-down (-up) quantized along the out-of-plane direction. The splitting in the conduction band is exaggerated. ω_u and ω_d are, respectively, the transition frequencies from the two split valence-band tops to the conduction band bottom. (c) Spin Hall effects of electrons and holes excited by linearly polarized optical field with frequency ω_u . (d) Valley Hall effects of electrons and holes excited by two-color optical fields with frequencies ω_u and ω_d and opposite circular polarizations.

Superconductivity in MoS₂

- Electro-static carrier doping was attempted in a layered MoS₂ by constructing an electric double-layer transistor with an ionic liquid.
- With the application of gate voltage V_G > 3V, a metallic behavior was observed in the MoS₂ channel.
- An onset of electric field-induced superconductivity was found in the field induced metallic phase. With a maximum T_C of 9.4K.
- APL, 101, 042603 (2012). Science, 350, 1353 (2015)

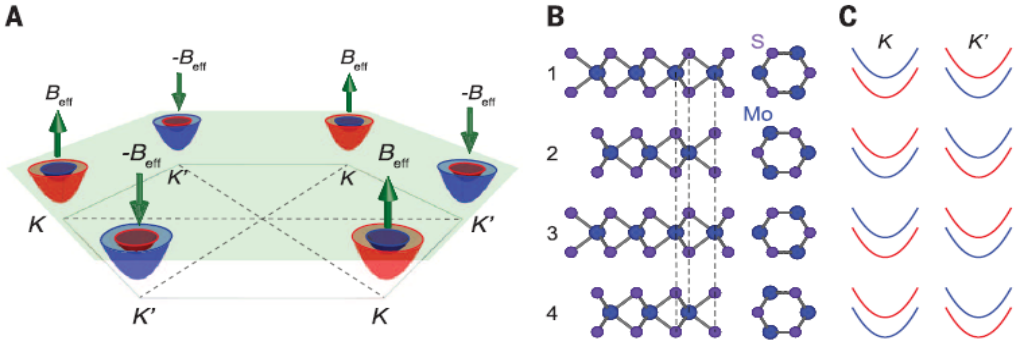
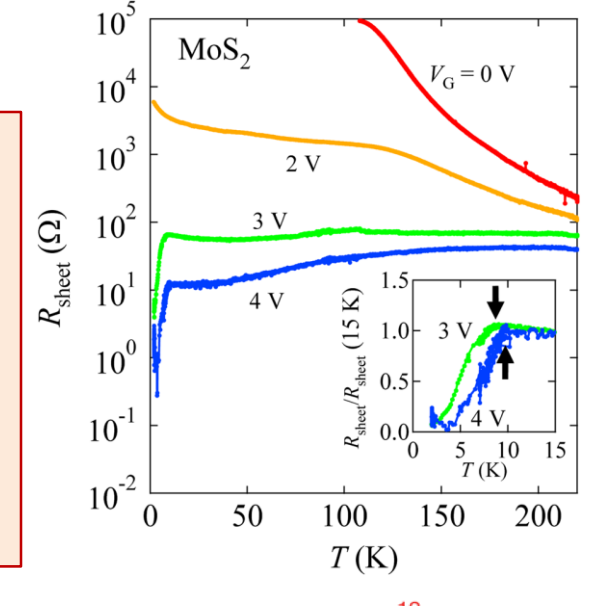
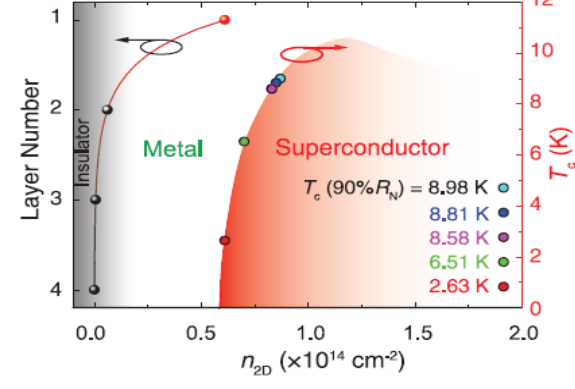


Fig. 1. Inducing superconductivity in thin flakes of MoS₂ by gating. (A) Conduction-band electron pockets near the K and K' points in the hexagonal Brillouin zone of monolayer MoS₂. Electrons in opposite K and K' points experience opposite effective magnetic fields \mathbf{B}_{eff} and $-\mathbf{B}_{\text{eff}}$, respectively (green arrows). The blue and red colored pockets indicate electron spins oriented up and down, respectively. (B) Side view (left) and top view (right) of the four outermost layers in a multilayered MoS₂ flake. The vertical dashed lines show the relative positions of Mo and S atoms in 2H-type stacking. In-plane inversion symmetry is broken in each individual layer, but global inversion symmetry is restored in bulk after stacking. (C) Energy-band splitting caused by Beff. Blue and red bands denote spins aligned up and down, respectively. Because of 2H-type stacking, adjacent layers have opposite \mathbf{B}_{eff} at the same K points. (D) The red curve (left axis) denotes the theoretical carrier density n_{2D} for the four outermost layers of MoS₂ (26) for sample D1, when $T_c(0) = 2.37$ K. In the phase diagram (right axis), superconducting states with different values of T_c(0) are color-coded; the same color-coding is used across all figures. Here, $T_{\rm c}$ is determined at the temperature where the resistance drop reaches 90% of R_N at 15 K. This criterion is different from the 50% R_N criterion used in the rest of the paper; it was chosen to be consistent with that used in the phase diagram of (17). (E) Temperature dependence of R_s, showing different values of T_c corresponding to superconducting states (from samples D1 and D24) denoted in (D).





D

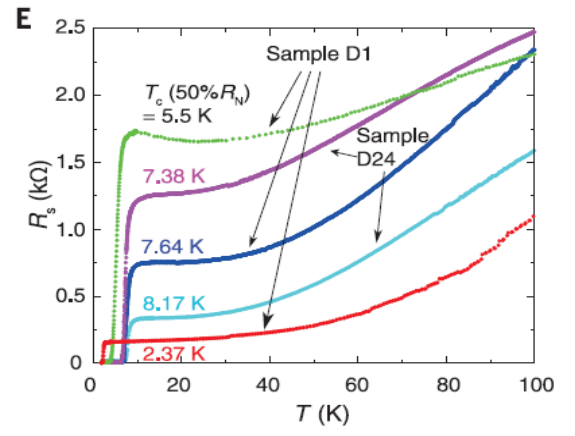
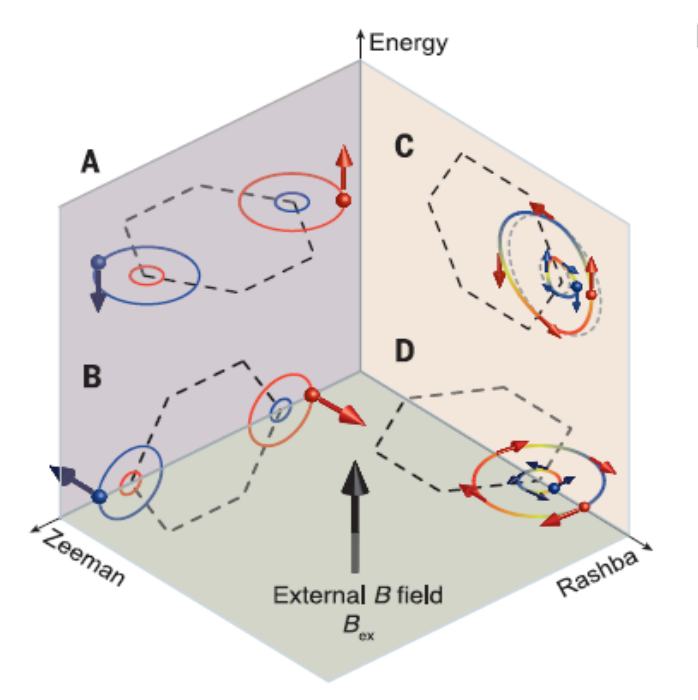
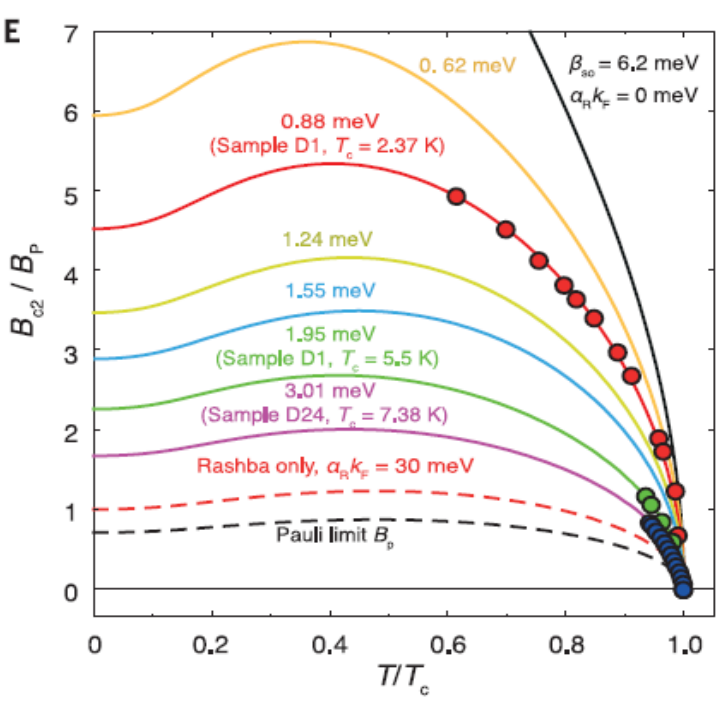
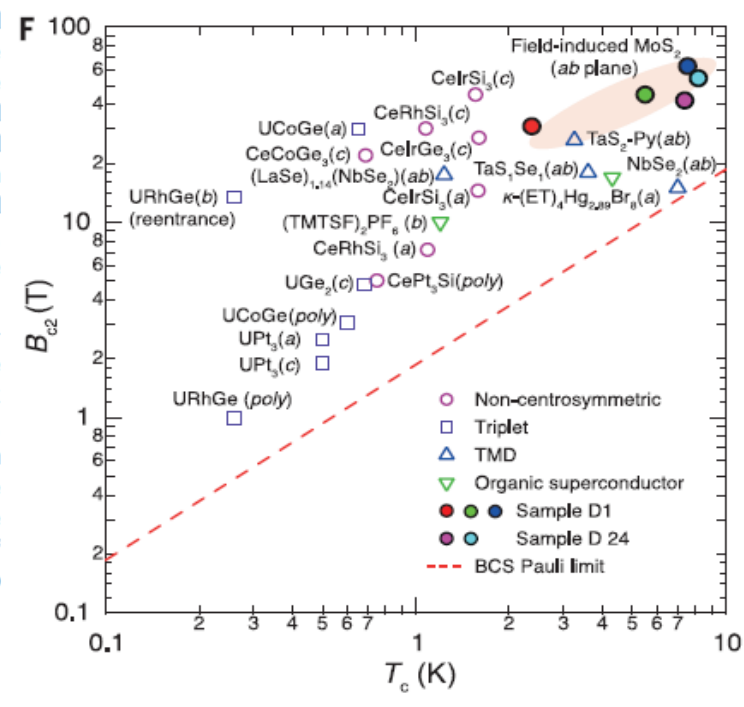


Fig. 4. Interplay between an external magnetic field and the spins of Cooper pairs aligned by Zeeman and Rashba-type effective magnetic fields. (A to D) Illustration of the acquisition of Zeeman energy through coupling between an external magnetic field and the spins of Cooper pairs formed near the K and K'points of the Brillouin zone (not to scale). When Rashba or Zeeman SOC aligns the spins of Cooper pairs parallel to the external field, the increase in Zeeman energy due to parallel



coupling between the field and the spin eventually can cause the pair to break [(A) and (C)]. In (B) and (D), the acquired Zeeman energy is minimized as a result of the orthogonal coupling between the field and the aligned spins, which effectively protects the Cooper pairs from depairing. (E) Theoretical fitting of the relationship between B_{c2}/B_{p} and T/T_c for samples D1 [$T_c(0) = 2.37$ K and 5.5 K] and D24 [$T_c(0) = 7.38$ K], using a fixed effective Zeeman field (β_{SO} = 6.2 meV) and an increasing Rashba field ($\alpha_R k_F$ ranges from 10 to ~50% of β_{SO}) [section 6 of (16)]. Two dashed lines show the special cases calculated by equation S3, when only the Rashba field ($\alpha_R k_F = 30 \text{ meV}$; $\beta_{SO} = 0$) is considered (red), and when both the Zeeman and Rashba fields are zero (black). In the former case, a large $\alpha_{\rm R}k_{\rm F}$ causes a moderate increase of $B_{\rm c2}$ to $\sim\sqrt{2}B_{\rm p}$ (10). In the latter case, the conventional Pauli limit at zero temperature is recovered. (F) Plot of B_{c2} versus T_c for different superconductors [a magnetic field was applied along crystal axes a, b, or c or to a polycrystalline (poly)]. The data shown are from well-known systems including noncentrosymmetric (pink circles), triplet (purple squares) (6, 8, 9), low-dimensional organic (green triangles) (40, 50-52), and bulk TMD superconductors (blue triangles) (35-38, 47). The robustness of the spin protection can be measured by the vertical distance between B_{c2} and the red dashed line denoting Bp. Gate-induced superconductivity from samples D1 and D24 are among the states with the highest B_{c2}/B_{p} ratio. In (LaSe)₁₁₄(NbSe₂), T_{c} was determined at 95% of R_N : T_c in organic molecule-intercalated TMDs was obtained by extrapolating to zero resistance; and all other systems use the standard of 50% of R_N.

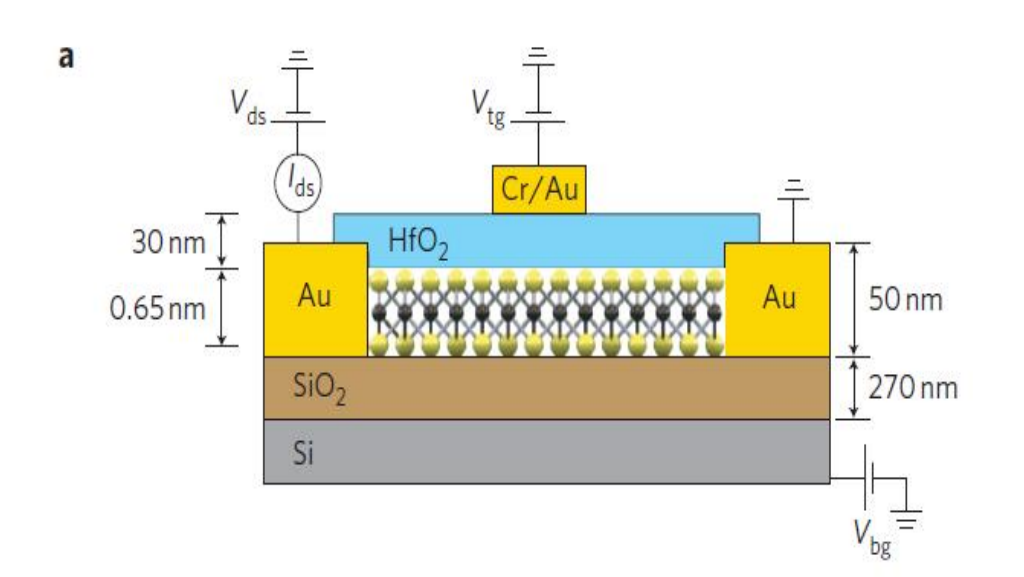


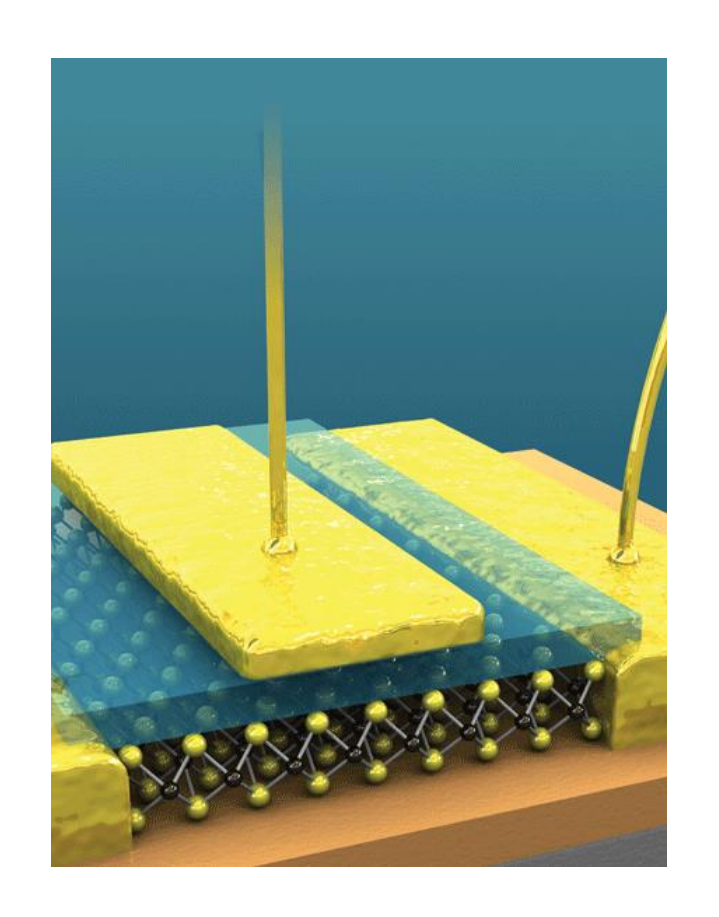


Field-effect transistors (FETs) based on MoS₂.

Andras Kis and co-workers have made an FET in which the channel is a single layer of MoS₂ that is just 0.65 nm thick and 1,500 nm long:

the black spheres in this schematic are Mo atoms; the yellow spheres are S atoms. The MoS_2 layer also has a bandgap, which is crucial for many applications.

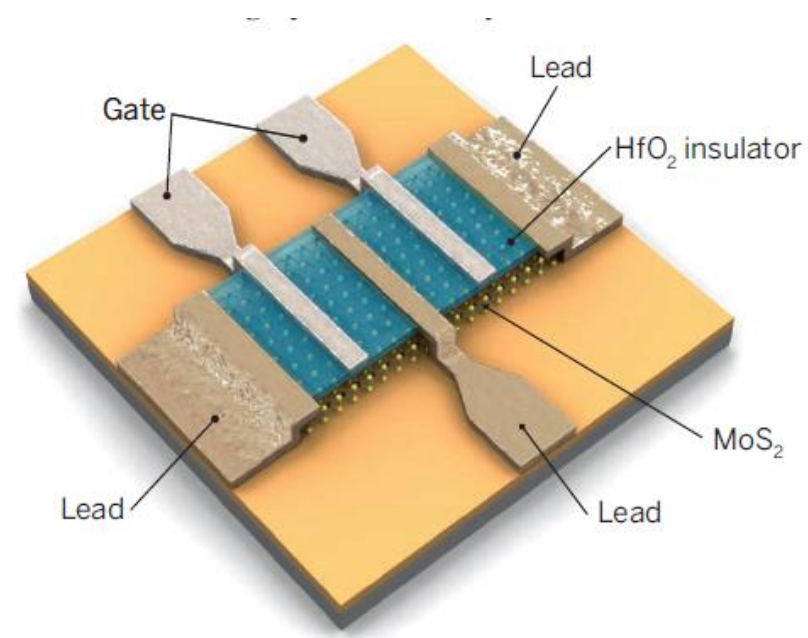




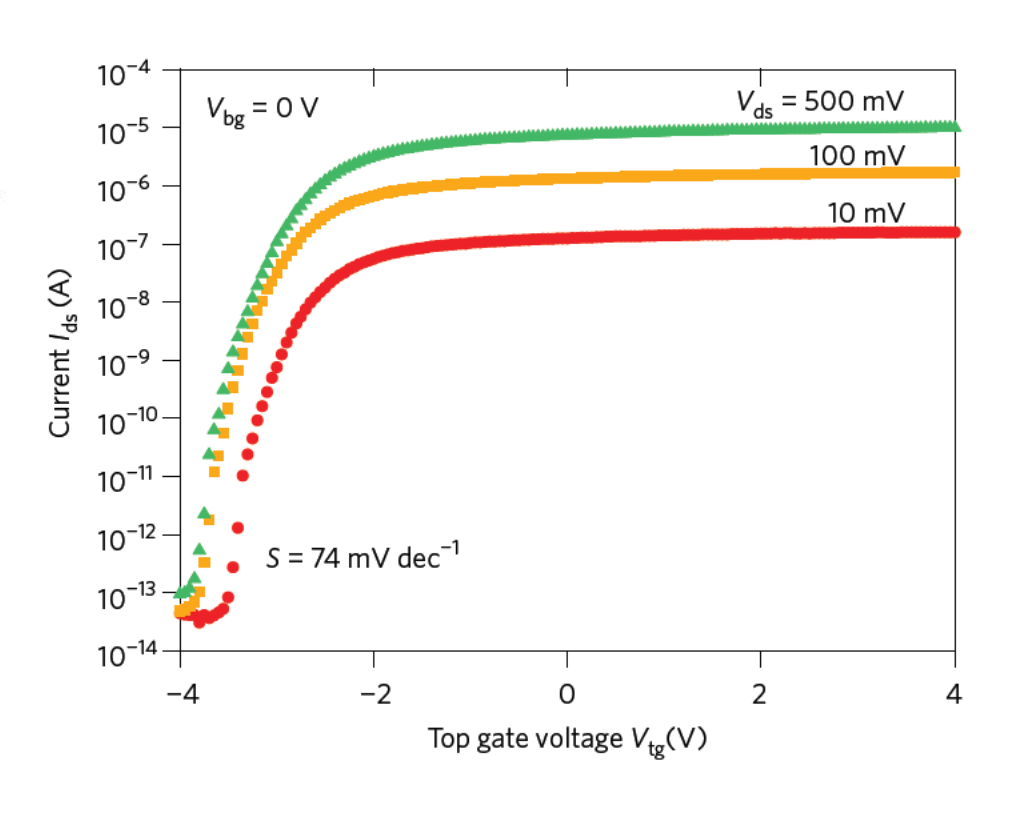
Andras Kis et al, Nature Nanotech. 6, No 3, 146, (2011).

MoS_2

- Switch on and off at 10⁹ times/sec, a large on/off ratio, making it easy to differentiate between digital 1s and 0s.
- A Mobility ~ 200; and was later corrected to ~15.



Researchers have made quick progress in turning 2D materials into devices, such as this simple circuit in which two transistors use MoS₂ to ferry charges between electrode leads.



Andras Kis, Nature Nanotechnology Vol 6, No 3, 146, (2011).

Field-Effect Mobility (review)

Monolayer MoS₂

- Room temperature mobility
- Back-gated Silicon oxide: 0.1 50 cm²/V.s SS: 1cm²/V.s
- Dual gate (SiO₂+HfO₂): **15** cm²/V sec
- Original ~200: Nat Nanotechnol 6, 147 (2011)
- Correction ~ 15: Nat Nanotechnol 8, 147 (2013)
- On/off ratio: 10⁸

Multilayer MoS₂

- Back-gated Al₂O₃: **100** cm²/Vsec
- multilayer MoS₂: 30nm
- On/off ratio: 10⁶

Nature Communications, 3, 1011 (2012)

• On PMMA: 470cm²/V.s(electrons)

480cm²/V.s(holes)

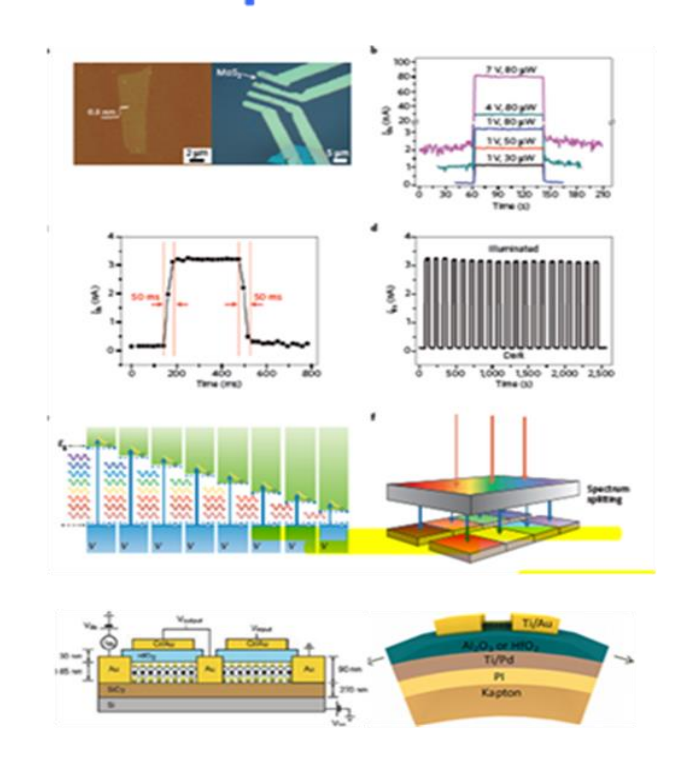
APL 102(4), 042104 (2013)

MoS₂ Optoelectronics

MoS₂'s strong interactions with light would be favorable for solar cells, light emitters, and other optical devices.

Optoelectronics Flexible Electronics Bendability Electronics MoS₂ Monolayer Hydrogen Production Valleytronics Battery New Physics

Flexible optoelectronics

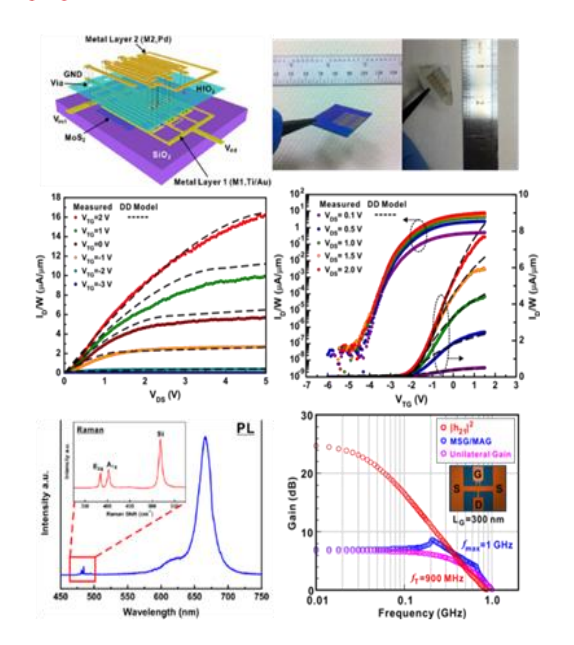


QH **Wang** et al, **Nat. Nano**, 7, p699 (2012)

Applications: Electronics

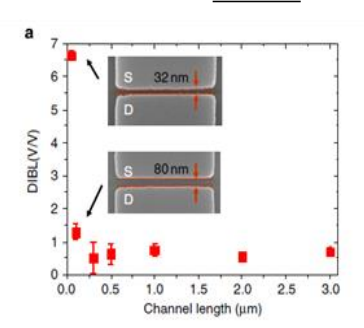
Large-scale CVD-MoS₂ Monolayer Devices:

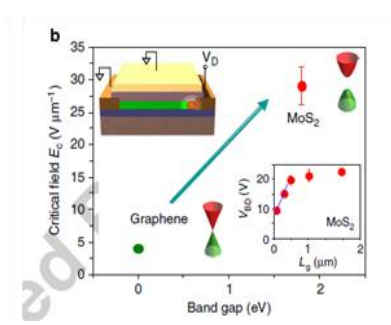
H. Wang, L. Yu, YH Lee et. al., *IEDM Tech. Digest*, 2012 -the best paper award in IEDM 2012



Electronic transport of CVD-MoS₂ Monolayer

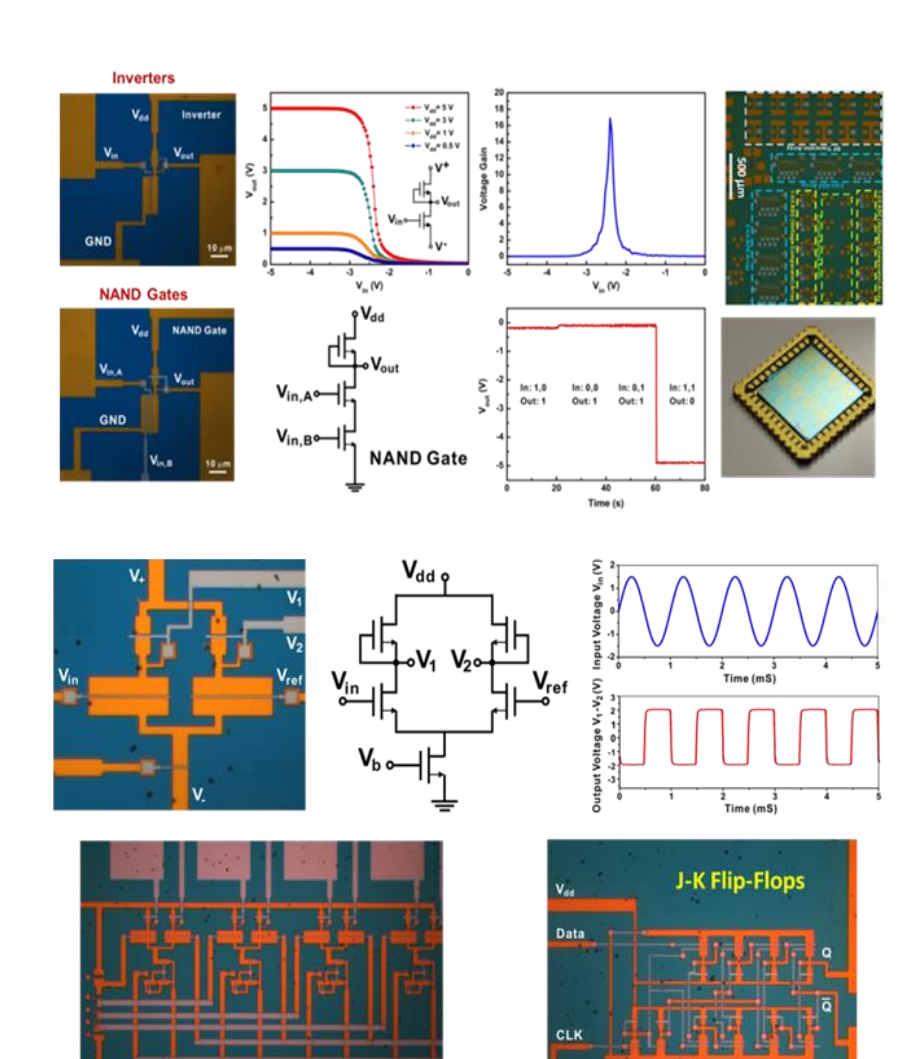
W. Zhu, and YH Lee et. al., Nat. Comm. 5,3087 (2014)





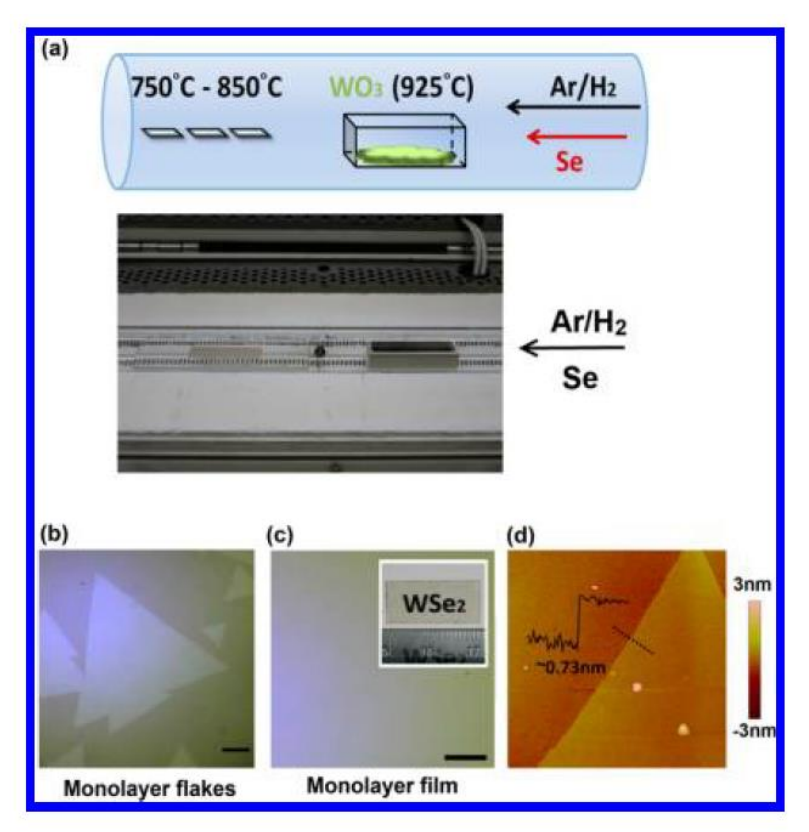
CVD-MoS₂ Monolayer Mixed-signal Circuits

H. Wang, YHLee et. al., (in-preparation)



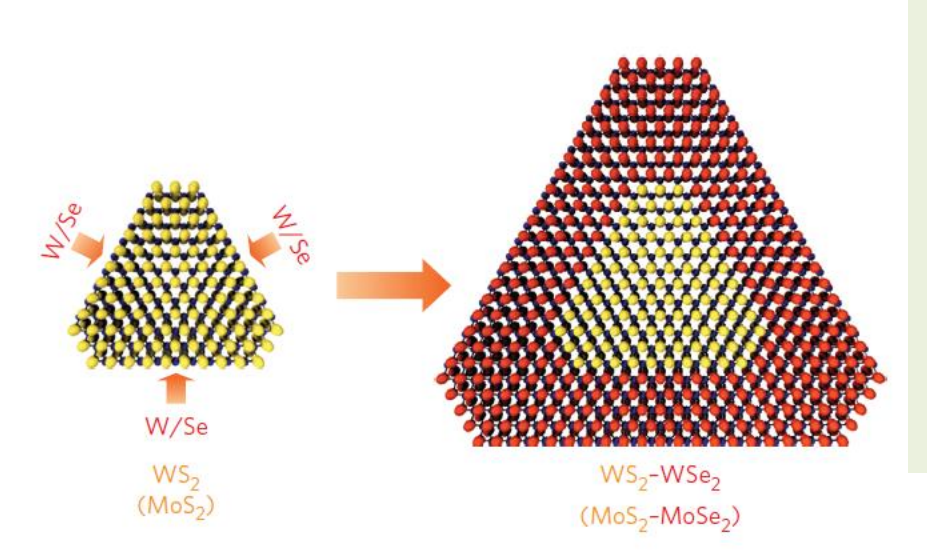
2-bit ADC

MoS₂ and WS₂ CVD growth



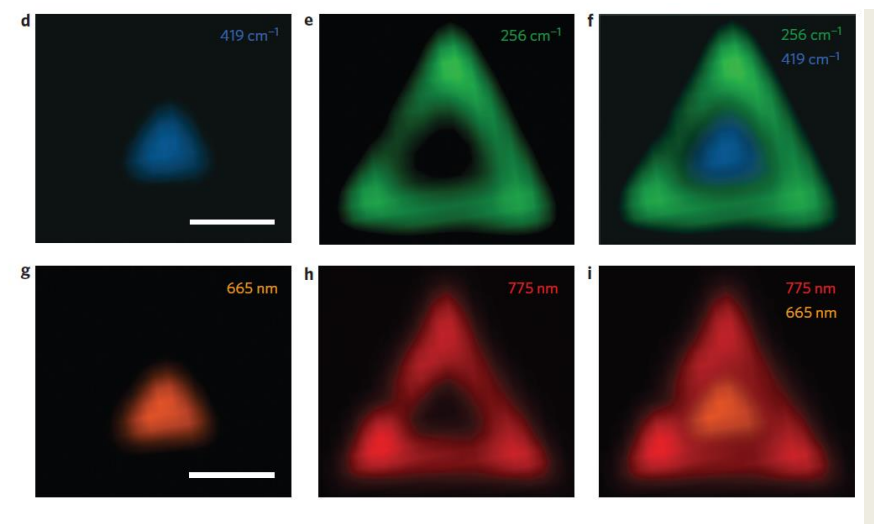
- (a) Schematic illustration for the growth of WSe₂ layers on sapphire substrates by the reaction of WO₃ and Se powders in a CVD furnace. A photo of the setup is also shown.
- (b) and (c) Optical microscopy images of the WSe_2 monolayer flakes and monolayer film grown at 850 and 750 C, respectively. Scale bar is 10 μ m in length. The inset in (c) shows the photograph of a uniform monolayer film grown on a double side polished sapphire substrate.
- (d) AFM image of a WSe₂ monolayer flake grown at 850 C on a sapphire substrate.

MoS₂ and WS₂ Lateral Epitaxy



Schematic of lateral epitaxial growth of WS₂–WSe₂ and MoS₂–MoSe₂ heterostructures.

- A triangular domain of WS₂ (MoS₂) is first grown using a CVD process.
- The peripheral edges of the triangular domain feature unsaturated dangling bonds that function as the active growth front for the continued addition, and incorporation of precursor atoms to extend the two dimensional crystal in the lateral direction.



NATURE NANOTECHNOLOGY, VOL 9, 1024, (2014).

d, Raman mapping at 419 cm–1 (WS $_2$ A1g signal), demonstrating that WS $_2$ is localized at the center region of the triangular domain. e, Raman mapping at 256 cm–1 (WSe2 A1g signal), demonstrating that WSe $_2$ is located in the peripheral region of the triangular domain. f, Composite image consisting of Raman mapping at 256 cm–1 and 419 cm–1, showing no apparent overlap or gap between the WS $_2$ and WSe $_2$ signals, demonstrating that the WS $_2$ inner triangle and WSe $_2$ peripheral areas are laterally connected. g,h, hotoluminescence mapping images at 665 nm and 775 nm, showing characteristic photoluminescence emission of WS $_2$ and WSe $_2$ in the center and peripheral regions of the triangular domain, respectively. i, Composite image consisting of photoluminescence mapping at 665 nm and 775 nm, demonstrating the formation of WS $_2$ –WSe $_2$ lateral heterostructures.

WSe₂-MoS₂ lateral p-n junction with an atomically sharp interface

